DOI: 10.17277/amt.2017.01.pp.044-055

Hybrid-Mixed Quadrilateral Element for Laminated Plates Composed of Functionally Graded Materials

G.M. Kulikov[1]*, E. Carrera[2], S.V. Plotnikova[1]

[1] *Laboratory of Intelligent Materials and Structures, Tambov State Technical University, 106, Sovetskaya St., Tambov, 392000, Russia*
[2] *Department of Aeronautics and Aerospace Engineering, Politecnico di Torino, 24, Corso Duca degli Abruzzi, Turin, 10129, Italy*

* Corresponding author. Tel.: + 7 (4752) 63 04 41. *E-mail*: gmkulikov@mail.ru

Abstract

A hybrid-mixed four-node quadrilateral element for the three-dimensional stress analysis of laminated functionally graded plates through the use of the method of sampling surfaces is developed. The sampling surfaces formulation is based on choosing inside the n^{th} layer I_n not equally spaced sampling surfaces parallel to the middle surface, in order to introduce the displacements of these surfaces as basic plate variables. The sampling surfaces are located inside each layer at Chebyshev polynomial nodes that allows one to uniformly minimize the error due to the Lagrange interpolation. To avoid shear locking and have no spurious zero energy modes, the assumed natural strain concept is employed. The developed assumed natural strain four-node quadrilateral plate element passes the bending patch tests for laminated and functionally graded plates and exhibits a superior performance in the case of coarse distorted mesh configurations. It can be useful for the three-dimensional stress analysis of thick and thin laminated functionally graded plates because the sampling surfaces formulation gives the possibility to obtain the numerical solutions with a prescribed accuracy, which asymptotically approach the three-dimensional exact solutions of elasticity as the number of sampling surfaces tends to infinity.

Keywords

Functionally graded material; hybrid-mixed quadrilateral element; laminated plate; sampling surfaces formulation; three-dimensional stress analysis.

Introduction

The functionally graded (**FG**) materials are a new class of advanced materials in which the material properties vary continuously from point to point. This property is achieved by varying the volume fraction of constituents. The FG materials are usually made by mixing the metal and ceramic phases. The ceramic with the low thermal conductivity serves as a thermal barrier and is placed at high temperature locations, whereas the metal is placed at regions where the mechanical properties such as toughness need to be high. The concept of the FG material was proposed by Japanese material scientists in the 1980s. However, most of the publications in the open literature appeared in the last fifteen years. The progress in the analytical and numerical modelling and analysis of FG materials and structures is reviewed in [1–3].

At present, the finite element method is widely used in bending, buckling and vibration analyses of FG plates and shells because of its advantages compared with other numerical techniques. The finite element formulations for the FG plates were developed in [4–7] through the first-order shear deformation theory [4] also known as a Reissner-Mindlin plate theory [5]. The major problem in constructing the low-order triangular and quadrilateral plate elements is how to eliminate shear locking for thin plates. The nodal integrated triangular and quadrilateral finite element formulation is presented in [6]. The proposed plate elements are free of locking and show little sensitivity to geometric distortions. The isogeometric finite

element formulation based on non-uniform rational B-splines (**NURBS**) was considered in [7]. It was established that shear locking can be overcome employing the NURBS functions of high order.

The finite element model for FG plates using the higher-order shear deformation theory was proposed by Reddy [8]. More general finite element formulations accounting for the transverse normal deformation for bending, buckling and free vibration analyses of FG plates are presented in [9, 10]. The nine-node rectangular plate element with 13 degrees of freedom (**DOFs)** per node has been developed in [9]. The NURBS-based finite element method for FG homogeneous and sandwich plates has been proposed in [10]. The feature of this approach is that only four displacement DOFs are utilized. The C^1-continuity requirement, however, can be carried out with the help of NURBS functions and no shear locking occurs.

Note that all finite elements considered do not describe well the through-thickness distribution of transverse stresses except for [11], where the efficient nine-node rectangular FG shell element with 15 DOFs per node has been developed via Carrera's fourth-order shell formulation [12, 13]. The shear and membrane locking phenomena are prevented through the assumed natural strain (**ANS)** method. However, the authors report that the transverse normal stress is calculated with a large error in the case of thin plates because of the small value of this stress compared to in-plane stresses.

The present paper is intended to overcome the above mentioned difficulties and develop the finite element that makes it possible to evaluate all stress components effectively for the thick and very thin FG plates. To solve such a problem, the four-node quadrilateral plate element using the sampling surfaces (**SaS**) technique [14, 15] is proposed. The SaS formulation is based on choosing inside the n^{th} layer the arbitrary number of surfaces $\Omega^{(n)1}, \Omega^{(n)2}, ..., \Omega^{(n)I_n}$ parallel to the middle surface in order to introduce the displacement vectors $\mathbf{u}^{(n)1}$, $\mathbf{u}^{(n)2}$,…, $\mathbf{u}^{(n)I_n}$ of these surfaces as basic plate variables, where I_n is the number of SaS of the n^{th} layer ($I_n \geq 3$). Such a choice of unknowns with the use of Lagrange polynomials of degree $I_n - 1$ in the assumed approximations of displacements, strains and material properties through the layer thicknesses leads to a very compact form of governing equations of the SaS laminated FG plate formulation. Recently, the SaS formulation has been utilized by Kulikov and Plotnikova to evaluate analytically the three-dimensional (**3D**) stress state in FG plates and shells [16–19].

In a proposed hybrid-mixed four-node finite element formulation, all SaS are located at Chebyshev polynomial nodes throughout the layers that make it possible to use the Lagrange polynomials of high degree [20]. To avoid shear locking and have no spurious zero energy modes in the case of distorted meshes, the assumed interpolations of displacement-independent strains and stress resultants in conjunction with the ANS interpolation of displacement-dependent transverse shear strains are utilized. To solve this problem, the Hu-Washizu multivariable variational principle is invoked. The developed isoparametric hybrid stress-strain finite element for the 3D stress analysis of laminated FG plates has computational advantages compared to the hybrid strain and hybrid stress finite elements. This is due to the fact that here no expensive numerical inversion of elemental matrices is needed; all matrix inversions can be done analytically. On the contrary, in conventional hybrid-mixed finite element formulations [21, 22] the inversion of the flexibility matrix is required. In fact, it is the most costly operation because the number of stress or strain parameters (modes) to be introduced to analyze effectively the laminated FG plates can be sufficiently large [23]. Note also that the proposed hybrid-mixed finite element model for the 3D stress analysis of laminated FG plates generalizes the authors' displacement-based finite element models [24, 25] and the hybrid-mixed quadrilateral four-node element models developed for single-layer and multilayered plates [26, 27] as well.

Three-Dimensional Description of Laminated Plate

Consider a laminated plate of the thickness h composed of N inhomogeneous layers. Let the middle surface Ω be described by Cartesian coordinates x_1 and x_2, whereas the coordinate x_3 is oriented in the thickness direction. The transverse coordinates of SaS of the n^{th} layer $x_3^{(n)i_n}$ are defined as

$$x_3^{(n)1} = x_3^{[n-1]}; \quad x_3^{(n)I_n} = x_3^{[n]}, \tag{1}$$

$$x_3^{(n)m_n} = \frac{1}{2}(x_3^{[n-1]} + x_3^{[n]}) - \frac{1}{2}h_n \cos\left(\pi \frac{2m_n - 3}{2(I_n - 2)}\right), \tag{2}$$

where $x_3^{[n-1]}$ and $x_3^{[n]}$ are the transverse coordinates of layer interfaces $\Omega^{[n-1]}$ and $\Omega^{[n]}$ depicted in Fig. 1; $h_n = x_3^{[n]} - x_3^{[n-1]}$ is the thickness of the n^{th} layer; I_n is the number of SaS corresponding to the n^{th} layer; the layer index n runs from 1 to N; the index m_n identifies the belonging of any quantity to the inner SaS of the n^{th} layer and runs from 2 to $I_n - 1$; the indices i_n, j_n, k_n are introduced for describing all SaS of the n^{th} layer and run from 1 to I_n; the Latin indices i, j, k, l range from 1 to 3; the Greek indices α, β range from 1 to 2.

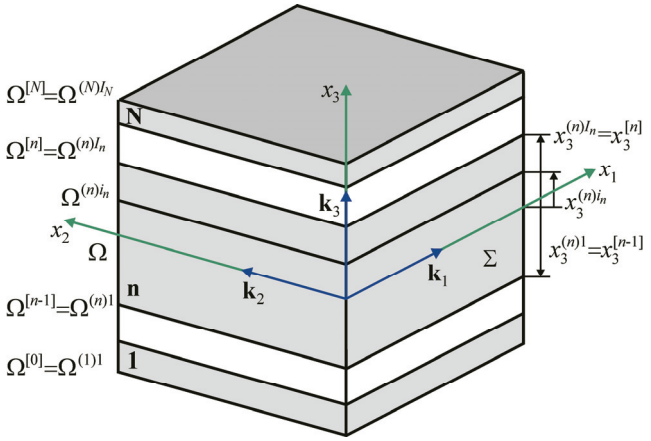

Fig. 1. Geometry of the laminated plate

It is important that the transverse coordinates of inner SaS (2) coincide with the coordinates of Chebyshev polynomial nodes [20]. This fact has a great meaning for the convergence characteristics of the SaS method [16–19].

The strains of the n^{th} layer $\varepsilon_{ij}^{(n)}$ can be written as

$$2\varepsilon_{ij}^{(n)} = u_{i,j}^{(n)} + u_{j,i}^{(n)}, \tag{3}$$

where $u_i^{(n)}$ are the displacements of the n^{th} layer.

Let us introduce the first two assumptions of the SaS laminated plate formulation. Assume that the displacements and strains are distributed through the thickness of the n^{th} layer as follows:

$$u_i^{(n)} = \sum_{i_n} L^{(n)i_n} u_i^{(n)i_n}; \quad u_i^{(n)i_n} = u_i^{(n)}(x_3^{(n)i_n}), \tag{4}$$

$$\varepsilon_{ij}^{(n)} = \sum_{i_n} L^{(n)i_n} \varepsilon_{ij}^{(n)i_n}; \quad \varepsilon_{ij}^{(n)i_n} = \varepsilon_{ij}^{(n)}(x_3^{(n)i_n}), \tag{5}$$

where $u_i^{(n)i_n}(x_1,x_2)$ are the displacements of SaS of the n^{th} layer $\Omega^{(n)i_n}$; $\varepsilon_{ij}^{(n)i_n}(x_1,x_2)$ are the strains of the same SaS; $L^{(n)i_n}(x_3)$ are the Lagrange polynomials of degree $I_n - 1$ defined as

$$L^{(n)i_n} = \prod_{j_n \neq i_n} \frac{x_3 - x_3^{(n)j_n}}{x_3^{(n)i_n} - x_3^{(n)j_n}}. \tag{6}$$

The use of (3)–(6) leads to relations between the SaS displacements and SaS strains:

$$2\varepsilon_{\alpha\beta}^{(n)i_n} = u_{\alpha,\beta}^{(n)i_n} + u_{\beta,\alpha}^{(n)i_n};$$

$$2\varepsilon_{\alpha 3}^{(n)i_n} = \beta_\alpha^{(n)i_n} + u_{3,\alpha}^{(n)i_n}; \quad \varepsilon_{33}^{(n)i_n} = \beta_3^{(n)i_n}, \tag{7}$$

where $\beta_i^{(n)i_n}(x_1,x_2)$ are the values of the derivatives of displacements with respect to the thickness coordinate at SaS given by

$$\beta_i^{(n)i_n} = u_{i,3}(x_3^{(n)i_n}) = \sum_{j_n} M^{(n)j_n}(x_3^{(n)i_n}) u_i^{(n)j_n}, \tag{8}$$

where $M^{(n)j_n} = L_{,3}^{(n)j_n}$ are the derivatives of Lagrange polynomials, which are calculated at SaS as

$$M^{(n)j_n}\left(x_3^{(n)i_n}\right) = \frac{1}{x_3^{(n)j_n} - x_3^{(n)i_n}} \prod_{k_n \neq i_n, j_n} \frac{x_3^{(n)i_n} - x_3^{(n)k_n}}{x_3^{(n)j_n} - x_3^{(n)k_n}}$$

for $j_n \neq i_n$,

$$M^{(n)i_n}\left(x_3^{(n)i_n}\right) = -\sum_{j_n \neq i_n} M^{(n)j_n}\left(x_3^{(n)i_n}\right). \tag{9}$$

It is seen from (8) that the key functions $\beta_i^{(n)i_n}$ of the SaS laminated plate formulation are represented as a linear combination of displacements of SaS of the n^{th} layer $u_i^{(n)j_n}$.

Hu-Washizu Mixed Variational Formulation for Laminated FG Plate

To develop the assumed stress-strain finite element formulation, we have to invoke the Hu-Washizu multi-field variational principle in which displacements, strains and stresses are utilized as independent variables [28]. It can be written as follows:

$$\delta J_{\text{HW}} = 0, \tag{10}$$

$$J_{\text{HW}} = \iint_\Omega \sum_n \int_{x_3^{[n-1]}}^{x_3^{[n]}} \left[\frac{1}{2} e_{ij}^{(n)} C_{ijkl}^{(n)} e_{kl}^{(n)} - \right.$$

$$\left. - \sigma_{ij}^{(n)}\left(e_{ij}^{(n)} - \varepsilon_{ij}^{(n)}\right)\right] dx_1 dx_2 dx_3 - W, \tag{11}$$

$$W = \iint_\Omega \left(p_i^+ u_i^+ - p_i^- u_i^-\right) dx_1 dx_2 + W_\Sigma,$$

where $\sigma_{ij}^{(n)}$ are the stresses of the n^{th} layer; $C_{ijkl}^{(n)}$ are the elastic constants of the n^{th} layer; $e_{ij}^{(n)}$ are the displacement-independent strains of the n^{th} layer; $u_i^- = u_i^{(1)1}$ and $u_i^+ = u_i^{(N)I_N}$ are the displacements of bottom and top surfaces; p_i^- and p_i^+ are the tractions acting on the bottom and top surfaces; W_Σ is the work done by external loads applied to the edge surface Σ. Here and in the following developments, the summation on repeated indices is implied.

Following the SaS technique, we introduce the third assumption of the proposed hybrid-stress finite element formulation. Let the displacement-independent strains be distributed through the thickness similar to displacement and displacement-dependent strain distributions (4) and (5), that is,

$$e_{ij}^{(n)} = \sum_{i_n} L^{(n)i_n} e_{ij}^{(n)i_n}; \quad e_{ij}^{(n)i_n} = e_{ij}^{(n)}(x_3^{(n)i_n}), \tag{12}$$

where $e_{ij}^{(n)i_n}(x_1,x_2)$ are the displacement-independent strains of SaS of the n^{th} layer.

Next, we introduce the last assumption of the SaS laminated FG plate formulation. Let the material constants of the n^{th} layer be distributed through the plate thickness as:

$$C_{ijkl}^{(n)} = \sum_{i_n} L^{(n)i_n} C_{ijkl}^{(n)i_n}; \quad C_{ijkl}^{(n)i_n} = C_{ijkl}^{(n)}(x_3^{(n)i_n}), \quad (13)$$

where $C_{ijkl}^{(n)i_n}(x_1, x_2)$ are the values of material constants of the n^{th} layer on SaS.

Substituting the through-thickness distributions (5), (12) and (13) into the Hu-Washizu variational principle (10) and (11), and introducing stress resultants

$$H_{ij}^{(n)i_n} = \int_{x_3^{[n-1]}}^{x_3^{[n]}} \sigma_{ij}^{(n)} L^{(n)i_n} dx_3, \quad (14)$$

the following variational equation is obtained:

$$\iint_\Omega \sum_n \sum_{i_n} \left[\delta\left(\mathbf{e}^{(n)i_n}\right)^{\mathrm{T}} \left(\mathbf{H}^{(n)i_n} - \sum_{j_n} \sum_{k_n} \Lambda^{(n)i_n j_n k_n} \mathbf{C}^{(n)j_n} \mathbf{e}^{(n)k_n} \right) + \right.$$
$$\left. + \delta\left(\mathbf{H}^{(n)i_n}\right)^{\mathrm{T}} \left(\mathbf{e}^{(n)i_n} - \boldsymbol{\varepsilon}^{(n)i_n}\right) - \delta\left(\boldsymbol{\varepsilon}^{(n)i_n}\right)^{\mathrm{T}} \mathbf{H}^{(n)i_n} \right] \mathrm{d}x_1 \mathrm{d}x_2 +$$
$$+ \int_\Omega \left(p_i^+ \delta u_i^+ - p_i^- \delta u_i^- \right) \mathrm{d}x_1 \mathrm{d}x_2 + \delta W_\Sigma = 0, \quad (15)$$

where

$$\boldsymbol{\varepsilon}^{(n)i_n} = \left[\varepsilon_{11}^{(n)i_n} \;\; \varepsilon_{22}^{(n)i_n} \;\; \varepsilon_{33}^{(n)i_n} \;\; 2\varepsilon_{12}^{(n)i_n} \;\; 2\varepsilon_{13}^{(n)i_n} \;\; 2\varepsilon_{23}^{(n)i_n} \right]^{\mathrm{T}};$$

$$\mathbf{e}^{(n)i_n} = \left[e_{11}^{(n)i_n} \;\; e_{22}^{(n)i_n} \;\; e_{33}^{(n)i_n} \;\; 2e_{12}^{(n)i_n} \;\; 2e_{13}^{(n)i_n} \;\; 2e_{23}^{(n)i_n} \right]^{\mathrm{T}};$$

$$\mathbf{H}^{(n)i_n} = \left[H_{11}^{(n)i_n} \;\; H_{22}^{(n)i_n} \;\; H_{33}^{(n)i_n} \;\; H_{12}^{(n)i_n} \;\; H_{13}^{(n)i_n} \;\; H_{23}^{(n)i_n} \right]^{\mathrm{T}};$$

$$\mathbf{C}^{(n)j_n} = \begin{bmatrix} C_{1111}^{(n)j_n} & C_{1122}^{(n)j_n} & C_{1133}^{(n)j_n} & C_{1112}^{(n)j_n} & 0 & 0 \\ C_{2211}^{(n)j_n} & C_{2222}^{(n)j_n} & C_{2233}^{(n)j_n} & C_{2212}^{(n)j_n} & 0 & 0 \\ C_{3311}^{(n)j_n} & C_{3322}^{(n)j_n} & C_{3333}^{(n)j_n} & C_{3312}^{(n)j_n} & 0 & 0 \\ C_{1211}^{(n)j_n} & C_{1222}^{(n)j_n} & C_{1233}^{(n)j_n} & C_{1212}^{(n)j_n} & 0 & 0 \\ 0 & 0 & 0 & 0 & C_{1313}^{(n)j_n} & C_{1323}^{(n)j_n} \\ 0 & 0 & 0 & 0 & C_{2313}^{(n)j_n} & C_{2323}^{(n)j_n} \end{bmatrix};$$

$$\Lambda^{(n)i_n j_n k_n} = \int_{x_3^{[n-1]}}^{x_3^{[n]}} L^{(n)i_n} L^{(n)j_n} L^{(n)k_n} dx_3. \quad (16)$$

Hybrid-Mixed ANS Finite Element Formulation

In the isoparametric four-node plate element formulation (from this point, Cartesian coordinates are denoted by x^1, x^2, x^3), the position vector and the displacement vector are approximated according to the standard °C interpolation:

$$x^\alpha = \sum_r N_r x_r^\alpha; \quad (17)$$

$$u_i^{(n)i_n} = \sum_r N_r u_{ir}^{(n)i_n}; \quad (18)$$

$$N_r = \frac{1}{4}\left(1 + n_{1r}\xi^1\right)\left(1 + n_{2r}\xi^2\right), \quad (19)$$

where $N_r\left(\xi^1, \xi^2\right)$ are the bilinear shape functions of the finite element with $n_{11} = n_{14} = n_{21} = n_{22} = 1$ and $n_{12} = n_{13} = n_{23} = n_{24} = -1$; x_r^α are the nodal coordinates; $u_{ir}^{(n)i_n}$ are the displacements of SaS at element nodes; the index r denotes the number of nodes and ranges from 1 to 4. The surface traction vector is also assumed to vary bilinearly throughout the element. The local numbering of the corner nodes and middle side nodes is shown in Fig. 2.

To overcome shear locking and have no spurious zero energy modes, the robust ANS interpolation [29, 30] of the transverse shear strains of SaS with four sampling points can be employed:

$$\varepsilon_{\alpha 3}^{(n)i_n} = \ell_\alpha^\beta \hat{\varepsilon}_{\beta 3}^{(n)i_n}; \quad (20)$$

$$\hat{\varepsilon}_{13}^{(n)i_n} = \frac{1}{2}\left(1 - \xi^2\right)\hat{\varepsilon}_{13}^{(n)i_n}(\mathrm{B}) + \frac{1}{2}\left(1 + \xi^2\right)\hat{\varepsilon}_{13}^{(n)i_n}(\mathrm{D}); \quad (21)$$

$$\hat{\varepsilon}_{23}^{(n)i_n} = \frac{1}{2}\left(1 - \xi^1\right)\hat{\varepsilon}_{23}^{(n)i_n}(\mathrm{A}) + \frac{1}{2}\left(1 + \xi^1\right)\hat{\varepsilon}_{23}^{(n)i_n}(\mathrm{C}), \quad (22)$$

where $\hat{\varepsilon}_{\alpha 3}^{(n)i_n}$ are the covariant components of the strain tensor of SaS in the contravariant basis $\boldsymbol{a}^\alpha = \ell_\beta^\alpha \mathrm{k}^\beta$, $\boldsymbol{a}^3 = \mathbf{k}_3$, which are defined by the orthogonality condition $\boldsymbol{a}_i \boldsymbol{a}^j = \delta_i^j$ (see Fig. 2).

The transverse shear strains $\hat{\varepsilon}_{\alpha 3}^{(n)i_n}$ at sampling points A, B, C and D are evaluated according to (7), (8) and (18) as:

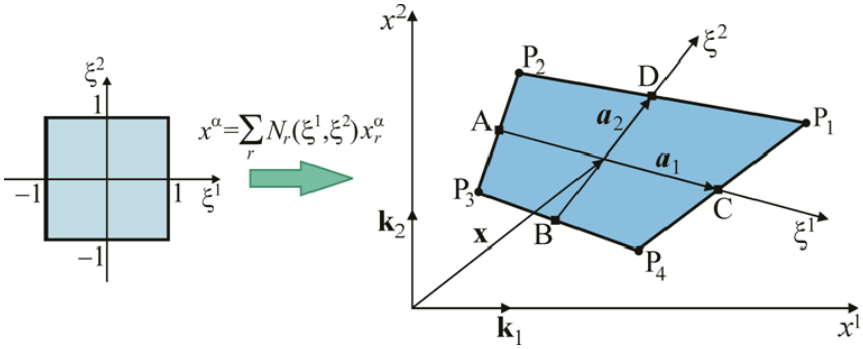

Fig. 2. Quadrilateral plate element

$$2\hat{\varepsilon}_{13}^{(n)i_n}(\mathrm{B})=\frac{1}{2}\left(u_{34}^{(n)i_n}-u_{33}^{(n)i_n}\right)+$$
$$+\frac{1}{4}\sum_{j_n}M^{(n)j_n}\left(z^{(n)i_n}\right)\left(x_4^{\alpha}-x_3^{\alpha}\right)\left(u_{\alpha 3}^{(n)j_n}+u_{\alpha 4}^{(n)j_n}\right);$$
$$2\hat{\varepsilon}_{13}^{(n)i_n}(\mathrm{D})=\frac{1}{2}\left(u_{31}^{(n)i_n}-u_{32}^{(n)i_n}\right)+$$
$$+\frac{1}{4}\sum_{j_n}M^{(n)j_n}\left(z^{(n)i_n}\right)\left(x_1^{\alpha}-x_2^{\alpha}\right)\left(u_{\alpha 1}^{(n)j_n}+u_{\alpha 2}^{(n)j_n}\right),;$$
$$2\hat{\varepsilon}_{23}^{(n)i_n}(\mathrm{A})=\frac{1}{2}\left(u_{32}^{(n)i_n}-u_{33}^{(n)i_n}\right)+$$
$$+\frac{1}{4}\sum_{j_n}M^{(n)j_n}\left(z^{(n)i_n}\right)\left(x_2^{\alpha}-x_3^{\alpha}\right)\left(u_{\alpha 2}^{(n)j_n}+u_{\alpha 3}^{(n)j_n}\right);$$
$$2\hat{\varepsilon}_{23}^{(n)i_n}(\mathrm{C})=\frac{1}{2}\left(u_{31}^{(n)i_n}-u_{34}^{(n)i_n}\right)+$$
$$+\frac{1}{4}\sum_{j_n}M^{(n)j_n}\left(z^{(n)i_n}\right)\left(x_1^{\alpha}-x_4^{\alpha}\right)\left(u_{\alpha 1}^{(n)j_n}+u_{\alpha 4}^{(n)j_n}\right), \quad (23)$$

where $z^{(n)i_n}$ stands for the transverse coordinates of SaS of the n^{th} layer $\Omega^{(n)i_n}$.

Substituting (18) in strain-displacement equations (7) and (8), and using the ANS interpolation (21)–(23) and presentation for the derivatives of shape functions

$$\begin{bmatrix}\frac{\partial N_r}{\partial x^1}\\ \frac{\partial N_r}{\partial x^2}\end{bmatrix}=\mathbf{J}^{-1}\begin{bmatrix}\frac{\partial N_r}{\partial \xi^1}\\ \frac{\partial N_r}{\partial \xi^2}\end{bmatrix}, \quad (24)$$

one obtains

$$\boldsymbol{\varepsilon}^{(n)i_n}=\mathbf{B}^{(n)i_n}\mathbf{U}, \quad (25)$$

where $\mathbf{J}^{-1}$ is the inverse Jacobian matrix; $\mathbf{B}^{(n)i_n}\left(\xi^1,\xi^2\right)$ are the strain-displacement transformation matrices of order 6×12 N_{SaS}; $N_{\text{SaS}}=\sum_n I_n-N+1$ is the total number of SaS; $\mathbf{U}$ is the element displacement vector given by:

$$\mathbf{U}=\left[\mathbf{U}_1^{\mathrm{T}}\ \mathbf{U}_2^{\mathrm{T}}\ \mathbf{U}_3^{\mathrm{T}}\ \mathbf{U}_4^{\mathrm{T}}\right]^{\mathrm{T}},$$
$$\mathbf{U}_r=\left[\left(\mathbf{u}_r^{[0]}\right)^{\mathrm{T}}\left(\mathbf{u}_r^{(1)2}\right)^{\mathrm{T}}\ldots\left(\mathbf{u}_r^{(1)I_1-1}\right)^{\mathrm{T}}\left(\mathbf{u}_r^{[1]}\right)^{\mathrm{T}}\left(\mathbf{u}_r^{(2)2}\right)^{\mathrm{T}}\ldots\right.$$
$$\left.\ldots\left(\mathbf{u}_r^{(N-1)I_{N-1}-1}\right)^{\mathrm{T}}\left(\mathbf{u}_r^{[N-1]}\right)^{\mathrm{T}}\left(\mathbf{u}_r^{(N)2}\right)^{\mathrm{T}}\ldots\left(\mathbf{u}_r^{(N)I_N-1}\right)^{\mathrm{T}}\left(\mathbf{u}_r^{[N]}\right)^{\mathrm{T}}\right]^{\mathrm{T}},$$
$$\mathbf{u}_r^{[m]}=\left[u_{1r}^{[m]}\ u_{2r}^{[m]}\ u_{3r}^{[m]}\right]^{\mathrm{T}}\quad (m=0,1,\ldots,N),$$
$$\mathbf{u}_r^{(n)m_n}=\left[u_{1r}^{(n)m_n}\ u_{2r}^{(n)m_n}\ u_{3r}^{(n)m_n}\right]^{\mathrm{T}}\quad (m_n=2,\ldots,I_n-1). \quad (26)$$

To improve the computational efficiency of the ANS four-node quadrilateral plate element, a hybrid-mixed method may be employed. In order to fulfill a patch test [31], the assumed stress resultants are interpolated throughout the element in the following form [26, 27]:

$$\mathbf{H}^{(n)i_n}=\mathbf{P}_{\sigma}\boldsymbol{\Phi}^{(n)i_n},\quad \boldsymbol{\Phi}^{(n)i_n}=\left[\Phi_1^{(n)i_n}\ \Phi_2^{(n)i_n}\ \ldots\ \Phi_{12}^{(n)i_n}\right]^{\mathrm{T}}, \quad (27)$$

$$\mathbf{P}_{\sigma}=\left[\mathbf{I}_6\ \overline{\mathbf{P}}_{\sigma}\right],$$
$$\overline{\mathbf{P}}_{\sigma}=\begin{bmatrix}\bar{t}_1^1\bar{t}_1^1\bar{\xi}^2 & \bar{t}_2^1\bar{t}_2^1\bar{\xi}^1 & 0 & 0 & 0 & 0\\ \bar{t}_1^2\bar{t}_1^2\bar{\xi}^2 & \bar{t}_2^2\bar{t}_2^2\bar{\xi}^1 & 0 & 0 & 0 & 0\\ 0 & 0 & \bar{\xi}^1 & \bar{\xi}^2 & 0 & 0\\ \bar{t}_1^1\bar{t}_1^2\bar{\xi}^2 & \bar{t}_2^1\bar{t}_2^2\bar{\xi}^1 & 0 & 0 & 0 & 0\\ 0 & 0 & 0 & 0 & \bar{t}_1^1\bar{\xi}^2 & \bar{t}_2^1\bar{\xi}^1\\ 0 & 0 & 0 & 0 & \bar{t}_1^2\bar{\xi}^2 & \bar{t}_2^2\bar{\xi}^1\end{bmatrix}, \quad (28)$$

where $\mathbf{I}_6$ is the unit matrix of order 6×6; $\bar{t}_{\alpha}^{\beta}$ are the elements of the Jacobian matrix $\mathbf{J}$ evaluated at the element center; $\bar{\xi}^{\alpha}$ are the transformed coordinates defined as:

$$\bar{t}_1^{\alpha}=\frac{1}{4}\left(x_1^{\alpha}-x_2^{\alpha}-x_3^{\alpha}+x_4^{\alpha}\right);\quad \bar{t}_2^{\alpha}=\frac{1}{4}\left(x_1^{\alpha}+x_2^{\alpha}-x_3^{\alpha}-x_4^{\alpha}\right);$$
$$\bar{\xi}^{\alpha}=\xi^{\alpha}-\xi_{\mathrm{c}}^{\alpha};\qquad \xi_{\mathrm{c}}^{\alpha}=\frac{1}{A_{\mathrm{el}}}\int_{-1}^{1}\int_{-1}^{1}\xi^{\alpha}\Delta\,\mathrm{d}\xi^1\mathrm{d}\xi^2;$$
$$A_{\mathrm{el}}=\int_{-1}^{1}\int_{-1}^{1}\Delta\,\mathrm{d}\xi^1\mathrm{d}\xi^2;\qquad \Delta=c_0+c_1\xi^1+c_2\xi^2;$$
$$c_0=\frac{1}{8}\left[\left(x_1^1-x_3^1\right)\left(x_2^2-x_4^2\right)-\left(x_2^1-x_4^1\right)\left(x_1^2-x_3^2\right)\right];$$
$$c_1=\frac{1}{8}\left[\left(x_1^1-x_2^1\right)\left(x_3^2-x_4^2\right)-\left(x_3^1-x_4^1\right)\left(x_1^2-x_2^2\right)\right];$$
$$c_2=\frac{1}{8}\left[\left(x_1^1-x_4^1\right)\left(x_2^2-x_3^2\right)-\left(x_2^1-x_3^1\right)\left(x_1^2-x_4^2\right)\right]. \quad (29)$$

The purpose of introducing $\bar{\xi}^{\alpha}$ lies in the simplicity of some elemental matrices of the hybrid-mixed method [32, 33] since

$$\int_{-1}^{1}\int_{-1}^{1}\bar{\xi}^{\alpha}\Delta\,\mathrm{d}\xi^1\mathrm{d}\xi^2=0. \quad (30)$$

The displacement-independent strains are interpolated throughout the element as suggested in [26, 27]:

$$\mathbf{e}^{(n)i_n}=\mathbf{P}_e\boldsymbol{\Psi}^{(n)i_n},\quad \boldsymbol{\Psi}^{(n)i_n}=\left[\Psi_1^{(n)i_n}\ \Psi_2^{(n)i_n}\ \ldots\ \Psi_{12}^{(n)i_n}\right]^{\mathrm{T}}, \quad (31)$$

$$\mathbf{P}_e = \left[\mathbf{I}_6 \ \overline{\mathbf{P}}_e\right],$$

$$\overline{\mathbf{P}}_e = \begin{bmatrix} \overline{\ell}_1^1\overline{\ell}_1^1\overline{\xi}^2 & \overline{\ell}_1^2\overline{\ell}_1^2\overline{\xi}^1 & 0 & 0 & 0 & 0 \\ \overline{\ell}_2^1\overline{\ell}_2^1\overline{\xi}^2 & \overline{\ell}_2^2\overline{\ell}_2^2\overline{\xi}^1 & 0 & 0 & 0 & 0 \\ 0 & 0 & \overline{\xi}^1 & \overline{\xi}^2 & 0 & 0 \\ 2\overline{\ell}_1^1\overline{\ell}_2^1\overline{\xi}^2 & 2\overline{\ell}_1^2\overline{\ell}_2^2\overline{\xi}^1 & 0 & 0 & 0 & 0 \\ 0 & 0 & 0 & 0 & \overline{\ell}_1^1\overline{\xi}^2 & \overline{\ell}_1^2\overline{\xi}^1 \\ 0 & 0 & 0 & 0 & \overline{\ell}_2^1\overline{\xi}^2 & \overline{\ell}_2^2\overline{\xi}^1 \end{bmatrix} \quad (32)$$

that corresponds to the interpolation of stress resultants (27), where $\overline{\ell}_\alpha^\beta$ are the elements of the inverse Jacobian matrix evaluated at the element center:

$$\overline{\ell}_1^1 = \frac{1}{c_0}\bar{t}_2^2, \ \ \overline{\ell}_1^2 = -\frac{1}{c_0}\bar{t}_1^2, \ \ \overline{\ell}_2^1 = -\frac{1}{c_0}\bar{t}_2^1, \ \ \overline{\ell}_2^2 = \frac{1}{c_0}\bar{t}_1^1. \quad (33)$$

Substituting interpolations (18), (25), (27) and (31) in the Hu-Washizu variational equation (15), we arrive at the element equilibrium equations:

$$\mathbf{Q}^{\mathrm{T}}\mathbf{\Phi}^{(n)i_n} = \sum_{j_n}\sum_{k_n}\Lambda^{(n)i_nj_nk_n}\mathbf{D}^{(n)j_n}\mathbf{\Psi}^{(n)k_n}, \quad (34)$$

$$\mathbf{Q}\mathbf{\Psi}^{(n)i_n} = \mathbf{R}^{(n)i_n}\mathbf{U}, \quad (35)$$

$$\sum_n\sum_{i_n}(\mathbf{R}^{(n)i_n})^{\mathrm{T}}\mathbf{\Phi}^{(n)i_n} = \mathbf{F}, \quad (36)$$

where $\mathbf{F}$ is the element-wise surface traction vector; $\mathbf{Q}$, $\mathbf{D}^{(n)j_n}$ and $\mathbf{R}^{(n)i_n}$ are the elemental matrices given by:

$$\mathbf{Q} = \int_{-1}^{1}\int_{-1}^{1}\mathbf{P}_\sigma^{\mathrm{T}}\mathbf{P}_e\Delta\,\mathrm{d}\xi^1\mathrm{d}\xi^2, \quad (37)$$

$$\mathbf{D}^{(n)j_n} = \int_{-1}^{1}\int_{-1}^{1}\mathbf{P}_e^{\mathrm{T}}\mathbf{C}^{(n)j_n}\mathbf{P}_e\Delta\,\mathrm{d}\xi^1\mathrm{d}\xi^2,$$
$$\mathbf{R}^{(n)i_n} = \int_{-1}^{1}\int_{-1}^{1}\mathbf{P}_\sigma^{\mathrm{T}}\mathbf{B}^{(n)i_n}\Delta\,\mathrm{d}\xi^1\mathrm{d}\xi^2. \quad (38)$$

The use of transformed coordinates $\overline{\xi}^\alpha$ in interpolations (27) and (31) is of great importance because the basic matrix of the hybrid stress-strain formulation $\mathbf{Q}$ becomes quasidiagonal:

$$\mathbf{Q} = A_{\mathrm{el}}\,\mathrm{diag}\left(\mathbf{I}_6, \omega_{22}, \omega_{11}, \begin{bmatrix}\omega_{11} & \omega_{12}\\ \omega_{12} & \omega_{22}\end{bmatrix}, \omega_{22}, \omega_{11}\right), \quad (39)$$

where

$$A_{\mathrm{el}} = 4c_0;$$

$$\omega_{\alpha\beta} = \frac{1}{A_{\mathrm{el}}}\int_{-1}^{1}\int_{-1}^{1}\overline{\xi}^\alpha\overline{\xi}^\beta\Delta\,\mathrm{d}\xi^1\mathrm{d}\xi^2 = \frac{1}{3}\left(\delta_{\alpha\beta} - \frac{c_\alpha c_\beta}{3c_0c_0}\right). \quad 40)$$

Due to interpolations (27), (28), (31) and (32) the stress resultants and displacement-independent strains are discontinuous at the element boundaries. Therefore, the column matrices $\mathbf{\Phi}^{(n)i_n}$ and $\mathbf{\Psi}^{(n)i_n}$ can be eliminated on the element level that yields finite element equations

$$\mathbf{K}\mathbf{U} = \mathbf{F}, \quad (41)$$

where $\mathbf{K}$ is the element stiffness matrix of order $12N_{\mathrm{SaS}}\times 12N_{\mathrm{SaS}}$ defined as

$$\mathbf{K} = \sum_n\sum_{i_n}\sum_{j_n}\sum_{k_n}\Lambda^{(n)i_nj_nk_n}\left(\mathbf{R}^{(n)i_n}\right)^{\mathrm{T}}\mathbf{Q}^{-1}\mathbf{D}^{(n)j_n}\mathbf{Q}^{-1}\mathbf{R}^{(n)k_n}. \quad (42)$$

Since the matrix $\mathbf{Q}$ is quasidiagonal, its inversion can be readily fulfilled in a closed form

$$\mathbf{Q}^{-1} = \frac{1}{A_{\mathrm{el}}}\mathrm{diag}\left(\mathbf{I}_6, 1/\omega_{22}, 1/\omega_{11}, \begin{bmatrix}\omega_{22}/d & -\omega_{12}/d\\ -\omega_{12}/d & \omega_{11}/d\end{bmatrix}, 1/\omega_{22}, 1/\omega_{11}\right), \quad (43)$$

where $d = \omega_{11}\omega_{22} - \omega_{12}\omega_{12}$. Thus, no expensive numerical inversion is needed if one uses the hybrid stress-strain quadrilateral plate formulation developed.

Remark 1. Because $L^{(n)i_n}$ are the Lagrange polynomials of degree $I_n - 1$ it is possible to carry out exact integration in (16) utilizing the Gaussian quadratures. Note also that the elemental matrices (38) are evaluated numerically through Gauss integration with 2×2 sampling points.

Remark 2. In a hybrid-mixed finite element formulation, the displacement-independent strains and stress resultants are selected so that the four-node quadrilateral plate element would be free of shear locking and kinematically stable. Owing to strain interpolation (31), we introduced 12 assumed strain parameters $\Psi_1^{(n)i_n}$, $\Psi_2^{(n)i_n}$,..., $\Psi_{12}^{(n)i_n}$ for each SaS, that is, $12N_{\mathrm{SaS}}$ for all SaS. It seems to be excessive recalling about $3N_{\mathrm{SaS}}$ DOFs per node. However, there exist six dependent strain modes exactly, which provide a correct rank of the element stiffness matrix [26].

Benchmark Problems

The performance of the proposed hybrid-mixed four-node laminated FG plate element denoted by SaSQP4 is evaluated with exact solutions of elasticity including 3D patch tests.

Bending patch test for laminated plate. The plate patch test for the bending behavior of quadrilateral elements confirms that the finite element formulation developed is able to reproduce the constant stress-strain states for distorted mesh configurations. Here, we consider a patch of five plate elements [34] with four external and four internal nodes as depicted in Fig. 3.

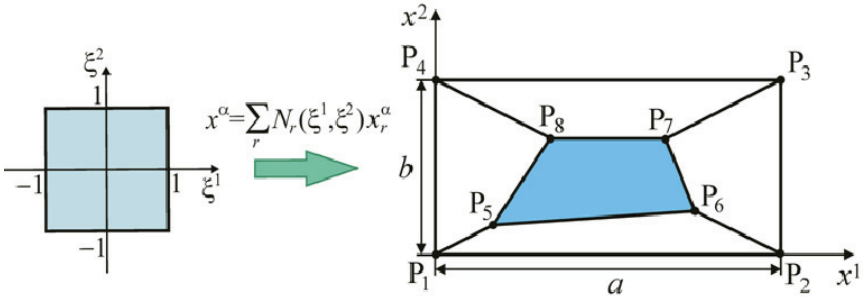

Coordinate	P_5	P_6	P_7	P_8
x^1	4	18	16	8
x^2	2	3	8	8

$a = 24,\ b = 12,\ h = 0.1$

Fig. 3. Patch test for a laminated FG plate

To achieve the constant 3D bending stress-strain state in the case of zero Poisson's ratios, the displacements of the n^{th} layer are chosen as:

$$u_1^{(n)} = ex^3\left(x^1 + \frac{1}{2}x^2\right);\quad u_2^{(n)} = ex^3\left(\frac{1}{2}x^1 + x^2\right);$$
$$u_3^{(n)} = -\frac{1}{2}e\left[\left(x^1\right)^2 + x^1x^2 + \left(x^2\right)^2\right]. \tag{44}$$

Inserting (44) in strain-displacement equations (3) and using constitutive equations, we arrive at the constant strain and stress fields in surfaces parallel to the middle surface:

$$\varepsilon_{11}^{(n)} = \varepsilon_{22}^{(n)} = ex^3;\quad 2\varepsilon_{12}^{(n)} = ex^3;\quad \varepsilon_{i3}^{(n)} = 0, \tag{45}$$

$$\sigma_{11}^{(n)} = \sigma_{22}^{(n)} = E_n ex^3;\quad \sigma_{12}^{(n)} = E_n ex^3/2;\quad \sigma_{i3}^{(n)} = 0, \tag{46}$$

where E_n is the elastic modulus of the n^{th} layer. One can verify that the equilibrium equations, continuity conditions at interfaces and boundary conditions on outer surfaces, which are free of tractions, are satisfied exactly.

Owing to 3D solution (44), the SaS displacements at exterior nodes can be prescribed as follows:

$$u_1^{(n)i_n} = ez^{(n)i_n}\left(x^1 + \frac{1}{2}x^2\right);\quad u_2^{(n)i_n} = ez^{(n)i_n}\left(\frac{1}{2}x^1 + x^2\right);$$
$$u_3^{(n)i_n} = -\frac{1}{2}e\left[\left(x^1\right)^2 + x^1x^2 + \left(x^2\right)^2\right] \tag{47}$$

that results in:

$$\varepsilon_{11}^{(n)i_n} = \varepsilon_{22}^{(n)i_n} = ez^{(n)i_n};\quad 2\varepsilon_{12}^{(n)i_n} = ez^{(n)i_n};$$
$$\varepsilon_{i3}^{(n)i_n} = 0. \tag{48}$$

As a numerical example, we consider a sandwich plate with $E_1 = E_3 = 10^7$; $E_2 = 10^5$; $h_1 = h_3 = h/10$; $h_2 = 8h/10$ and $e = 10^{-5}$. Applying the prescribed displacements (47) to exterior nodes, one can observe that the displacements and strains at interior nodes are identical to analytical answers. This is partially confirmed by displacements of the top surface u_i^+ at interior nodes listed in Table 1 for three and five SaS inside each layer. Thus, the SaSQP4 element passes the bending plate patch test for a sandwich plate. It should be mentioned that the computations were performed employing the 16-digit calculation.

Bending patch test for FG plate. Consider again a patch of five plate elements shown in Fig. 3. The elastic modulus is assumed to be distributed through the thickness of the plate according to the exponential law

$$E = E^- e^{\alpha(z+0.5)};\quad -0.5 \le z \le 0.5, \tag{49}$$

where E^- is the elastic modulus on the bottom surface; $z = x_3/h$ is the dimensionless thickness coordinate; α is the material gradient index defined as

$$\alpha = \ln\left(E^+/E^-\right), \tag{50}$$

where E^+ is the elastic modulus on the top surface.

Applying the SaS displacements (47) for $n = 1$ to exterior nodes of the plate with $E^- = 10^6$, $\alpha = 2$ and $e = 10^{-5}$, one can conclude that the SaSQP4 element passes the bending patch test for a FG plate as well. It is seen from Table 2, where displacements of the top surface at interior nodes for three and seven SaS are presented.

Table 1

Displacements at interior nodes in the bending patch test for a sandwich plate

Formulation	Node	$10^6 \cdot u_1^+$	$10^6 \cdot u_2^+$	$-10^4 \cdot u_3^+$
Exact values	P_5	2.500000	2.000000	1.400000
	P_6	9.750000	6.000000	19.35000
	P_7	10.00000	8.000000	22.40000
	P_8	6.000000	6.000000	9.600000
$I_n = 3$	P_5	2.500013	2.000003	1.400006
	P_6	9.749988	6.000002	19.35001
	P_7	9.999981	8.000001	22.40002
	P_8	6.000017	5.999995	9.600016
$I_n = 5$	P_5	2.499885	2.000125	1.399982
	P_6	9.750077	5.999927	19.34993
	P_7	9.999878	8.000213	22.40000
	P_8	6.000069	6.000015	9.600048

Table 2

Displacements at interior nodes in the bending patch test for a FG plate

Formulation	Node	$10^6 \cdot u_1^+$	$10^6 \cdot u_2^+$	$-10^4 \cdot u_3^+$
Exact values	P_5	2.5000000	2.0000000	1.4000000
	P_6	9.7500000	6.0000000	19.350000
	P_7	10.000000	8.0000000	22.400000
	P_8	6.0000000	6.0000000	9.6000000
$I_1 = 3$	P_5	2.4999924	1.9999993	1.3999954
	P_6	9.7500068	5.9999996	19.349998
	P_7	10.000003	8.0000001	22.399997
	P_8	5.9999974	6.0000007	9.5999966
$I_1 = 7$	P_5	2.4999924	1.9999993	1.3999954
	P_6	9.7500068	5.9999982	19.349993
	P_7	10.000010	8.0000009	22.399988
	P_8	5.9999903	6.0000028	9.5999871

Simply supported three-layer FG rectangular plate under sinusoidal loading. Here, we study a three-layer rectangular plate subjected to sinusoidally distributed transverse loading acting on its top surface

$$p_3^+ = p_0 \sin\frac{\pi x^1}{a}\sin\frac{\pi x^2}{b}, \quad p_3^- = 0, \tag{51}$$

where a and b are the length and width of the plate.

The bottom and top layers with equal thicknesses $h_1 = h_3 = h/4$, are composed of the graphite-epoxy composite with the material properties

$E_L = 172.72$ GPa, $E_T = 6.909$ GPa, $G_{LT} = 3.45$ GPa, $G_{TT} = 1.38$ GPa, and $\nu_{LT} = \nu_{TT} = 0.25$. It is assumed that the fibers of bottom and top layers are oriented respectively in x^1- and x^2-directions. The central layer of the thickness $h_2 = h/2$ is made of the transversely isotropic FG material with the elastic constants distributed through the thickness according to a power law:

$$C_{ijkl} = C_{ijkl}^- V^- + C_{ijkl}^+ V^+,$$
$$V^+ = 1 - V^-, \quad V^- = (0.5 - 2z)^\gamma, \tag{52}$$
$$-0.25 \le z \le 0.25,$$

where C_{ijkl}^- and C_{ijkl}^+ are the values of elastic constants on both interfaces; γ is the material gradient index; $z = x_3/h$ is the dimensionless thickness coordinate. The elastic constants on the bottom interface are considered to be the same as those in [16]:

$$C_{1111}^- = C_{2222}^- = 41.3 \text{ GPa}; \quad C_{1122}^- = 14.7 \text{ GPa};$$
$$C_{1133}^- = C_{2233}^- = 10.1 \text{ GPa};$$
$$C_{3333}^- = 36.2 \text{ GPa}; \quad C_{1313}^- = C_{2323}^- = 10.0 \text{ GPa};$$
$$C_{1212}^- = 13.3 \text{ GPa},$$

whereas the elastic constants on the top interface are taken as $C_{ijkl}^+ = 2C_{ijkl}^-$.

To analyze efficiently the results obtained for $\gamma = 2$, we introduce the dimensionless displacements and stresses at crucial points as functions of the thickness coordinate:

$$\bar{u}_1 = E_L u_1(a, b/2, z)/hp_0; \quad \bar{u}_2 = E_L u_2(a/2, b, z)/hp_0;$$
$$\bar{u}_3 = E_L u_3(a/2, b/2, z)/hp_0;$$
$$\bar{\sigma}_{11} = \sigma_{11}(a/2, b/2, z)/p_0; \quad \bar{\sigma}_{22} = \sigma_{22}(a/2, b/2, z)/p_0;$$
$$\bar{\sigma}_{12} = \sigma_{12}(a, b, z)/p_0;$$
$$\bar{\sigma}_{13} = \sigma_{13}(a, b/2, z)/p_0; \quad \bar{\sigma}_{23} = \sigma_{23}(a/2, b, z)/p_0;$$
$$\bar{\sigma}_{33} = \sigma_{33}(a/2, b/2, z)/p_0,$$

where $a = b = 1m$.

Due to symmetry of the problem, only one quarter of the plate (see Fig. 4) is modeled by a uniform 64×64 mesh of SaSQP4 elements. The data listed in Tables 3 and 4 show that the SaSQP4 element allows reproducing the authors' exact SaS solution [16] for thick and moderately thick plates with a high accuracy using the sufficiently large number of SaS inside the layers. As can be seen, the SaSQP4 element provides from three to four right digits for the displacements and stresses at crucial points.

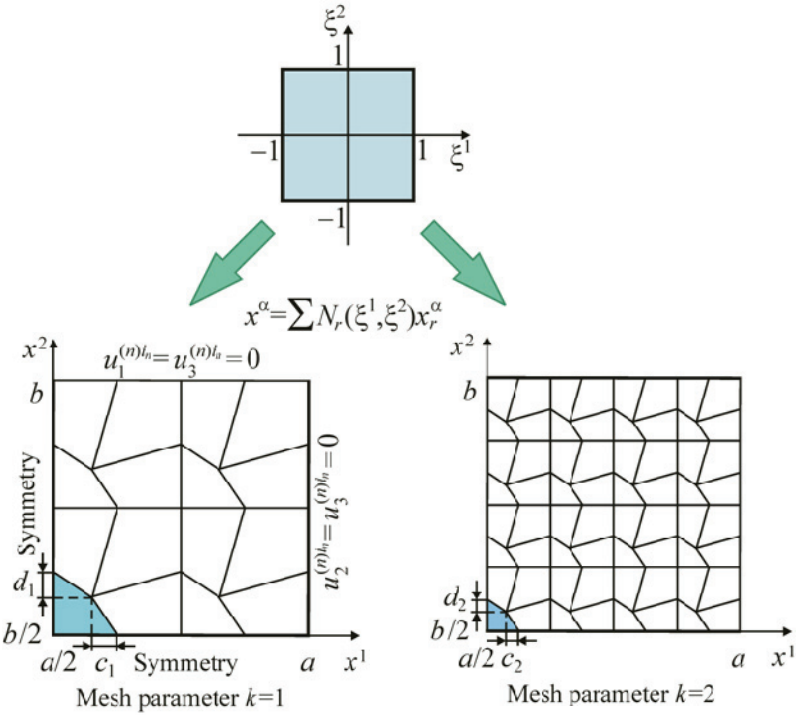

Fig. 4. One quarter of the simply supported three-layer FG rectangular plate modeled by distorted $4k \times 4k$ meshes with $c_k = \delta a/8k$ and $d_k = \delta b/8k$, where $k = 1,2, \ldots, 16$ and $\delta \in [0, 0.6]$

Table 3

Convergence study for a three-layer plate with $a/h = 2$ using a uniform 64×64 mesh

Formulation	$\bar{u}_1(0.5)$	$\bar{u}_2(0.5)$	$\bar{u}_3(0.5)$	$\bar{\sigma}_{11}(0.5)$	$\bar{\sigma}_{22}(0.5)$	$\bar{\sigma}_{12}(0.5)$	$\bar{\sigma}_{13}(0)$	$\bar{\sigma}_{23}(0)$	$\bar{\sigma}_{33}(0)$
$I_n = 3$	3.1523	1.3399	12.772	0.48238	2.4846	–0.14093	–0.55566	–0.49464	0.43906
$I_n = 4$	3.1999	1.3734	12.832	0.47708	2.5271	–0.14347	–0.60492	–0.55892	0.44618
$I_n = 5$	3.2013	1.3769	12.836	0.47684	2.5322	–0.14363	–0.61857	–0.57944	0.45233
$I_n = 6$	3.2014	1.3769	12.836	0.47643	2.5317	–0.14363	–0.61815	–0.57703	0.45162
Exact [16]	3.2012	–	12.835	0.47646	2.5318	–0.14364	–0.61797	–0.57637	0.45156

Table 4

Convergence study for a three-layer plate with $a/h = 10$ using a uniform 64×64 mesh

Formulation	$\bar{u}_1(0.5)$	$\bar{u}_2(0.5)$	$\bar{u}_3(0.5)$	$\bar{\sigma}_{11}(0.5)$	$\bar{\sigma}_{22}(0.5)$	$\bar{\sigma}_{12}(0.5)$	$\bar{\sigma}_{13}(0)$	$\bar{\sigma}_{23}(0)$	$\bar{\sigma}_{33}(0)$
$I_n = 3$	418.71	143.34	1969.8	5.9872	46.781	–3.5266	–2.8096	–2.2369	0.48776
$I_n = 4$	418.95	143.42	1970.7	5.9834	46.798	–3.5286	–2.9218	–2.4611	0.50103
$I_n = 5$	418.95	143.42	1970.7	5.9823	46.798	–3.5286	–2.9551	–2.5383	0.50483
$I_n = 6$	418.95	143.42	1970.7	5.9823	46.797	–3.5286	–2.9635	–2.5339	0.50420
Exact [16]	418.93	–	1970.7	5.9825	46.799	–3.5288	–2.9655	–2.5329	0.50436

Figure 5 displays the distributions of stresses through the thickness of the three-layer FG plate for different values of the slenderness ratio a/h by choosing five SaS and the same fine finite element mesh. These results demonstrate convincingly the high potential of the SaSQP4 element developed because the boundary conditions on bottom and top surfaces and the continuity conditions at interfaces for transverse stresses are satisfied correctly.

To investigate the performance of the SaSQP4 element more carefully, we consider the distorted $4k \times 4k$ finite element meshes composed of $2k \times 2k$

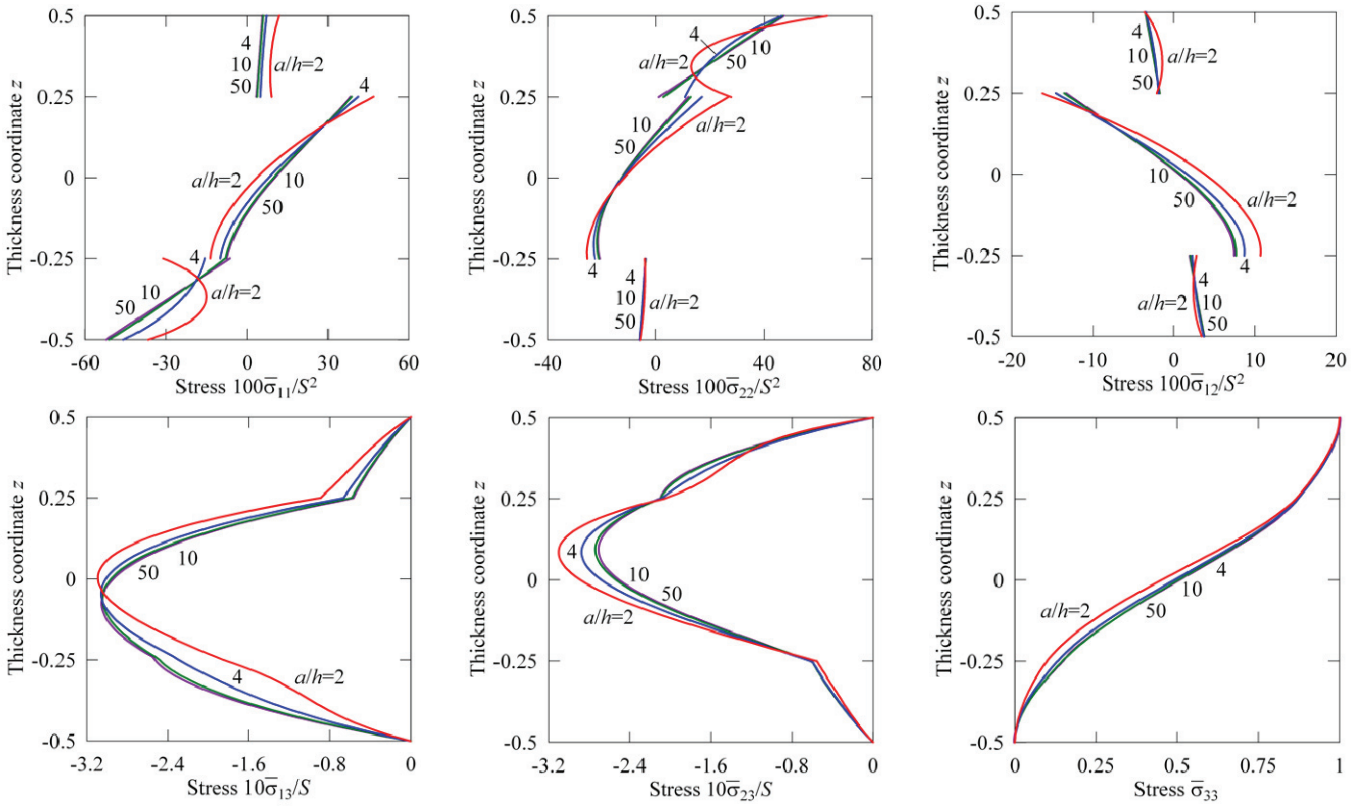

Fig. 5. Through-thickness distributions of stresses of the simply supported three-layer FG square plate with $I_1 = I_2 = I_3 = 5$ using a uniform 64×64 mesh, where $S = a/h$

squares with distorted 2×2 meshes inside them as depicted in Fig. 4. The element mesh inside each square is distorted by moving the inner node along the diagonal. As a result, the generated meshes are defined by distortion parameters $c_k = \delta a/8k$ and $d_k = \delta b/8k$, which are dependent on a single distortion parameter $\delta \in [0, 0.6]$. Figures 6 *a*, *b* show the results of the convergence study due to mesh refinement and mesh

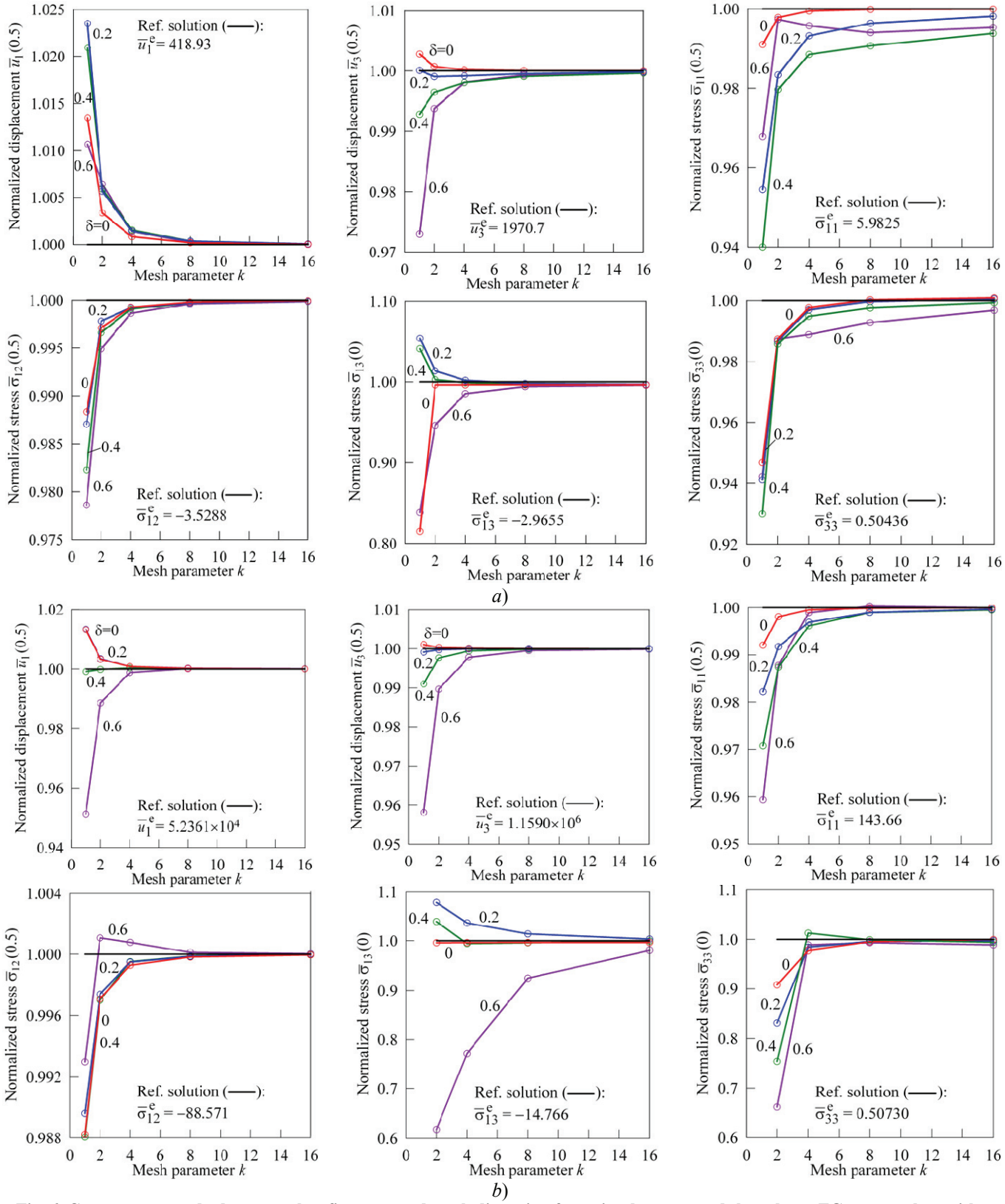

Fig. 6. Convergence study due to mesh refinement and mesh distortion for a simply supported three-layer FG square plate with: *a* – $a/h = 10$ and $I_1 = I_2 = I_3 = 5$; *b* – $a/h = 50$ and $I_1 = I_2 = I_3 = 5$

distortion through the use of normalized displacements and stresses for slenderness ratios of 10 and 50 by choosing five SaS inside each layer. The analytical answers are provided by the exact SaS solution [16]. It is seen that the SaSQP4 element behaves practically insensitive with respect to the extremely high mesh distortion including $\delta = 0.6$ except for transverse stresses in the case of thin plates.

Conclusion

The paper describes a hybrid-mixed ANS four-node quadrilateral laminated FG plate element based on the SaS formulation in which the displacements of SaS are utilized as basic plate unknowns. The SaS are located at Chebyshev polynomial nodes inside the plate body that make it possible to minimize uniformly the error due to Lagrange interpolation of displacements, strains and material properties through the layer thicknesses. The element stiffness matrix is evaluated without using the expensive numerical matrix inversion that is impossible in available hybrid-mixed finite element formulations. The quadrilateral element developed passes 3D bending patch tests for laminated and FG plates. It can be recommended for the 3D stress analysis of thin and thick laminated FG plates due to the fact that the SaS solutions asymptotically approach the solutions of elasticity as the number of SaS goes to infinity.

Acknowledgements

This work was supported by the Russian Science Foundation (Grant No. 15-19-30002) and the Russian Ministry of Education and Science (Grant No. 9.4914.2017).

References

1. Birman, V., & Byrd, L.W. Modeling and analysis of functionally graded materials and structures. *Applied Mechanical Review*, 2007, vol. 60, pp. 195-216.

2. Jha, D.K., Kant, T., Singh, R.K. A critical review of recent research on functionally graded plates. *Composite Structures*, 2013, vol. 96, pp. 833-849.

3. Swaminathan, K., Naveenkumar, D.T., Zenkour, A.M., Carrera, E. Stress, vibration and buckling analyses of FGM plates – A state-of-the-art review. *Composite Structures*, 2015, vol. 120, pp. 10-31.

4. Praveen, G., Reddy, J.N. Nonlinear transient thermoelastic analysis of functionally graded ceramic-metal plates. *International Journal of Solids and Structures*, 1998, vol. 35, pp. 4457-4476.

5. Croce, L.D., Venini, P. Finite elements for functionally graded Reissner-Mindlin plates. *Computer Methods in Applied Mechanics and Engineering*, 2004, vol. 193, pp. 705-725.

6. Castellazzi, G., Gentilini, C., Krysl, P., Elishakoff, I. Static analysis of functionally graded plates using a nodal integrated finite element approach. *Composite Structures*, 2013, vol. 103, pp. 197-200.

7. Valizadeh, N., Natarajan, S., Gonzalez-Estrada, O.A., Rabczuk, T., Bui, T.Q., Bordas, S.P.A. NURBS-based finite element analysis of functionally graded plates: Static bending, vibration, buckling and flutter. *Composite Structures*, 2013, vol. 99, pp. 309-326.

8. Reddy, J.N. Analysis of functionally graded plates. *International Journal for Numerical Methods in Engineering*, 2000, vol. 47, pp. 663-684.

9. Talha, M., Singh, B.N. Static response and free vibration analysis of FGM plates using higher order shear deformation theory. *Applied Mathematical Modelling*, 2010, vol. 34, pp. 3991-4011.

10. Thai, C.H., Zenkour, A.M., Wahab, M.A., Nguyen-Xuan, H. A simple four-unknown shear and normal deformations theory for functionally graded isotropic and sandwich plates based on isogeometric analysis. *Composite Structures*, 2016, vol. 139, pp. 77-95.

11. Cinefra, M., Carrera, E., Croce, L.D., Chinosi, C. Refined shell elements for the analysis of functionally graded structures. *Composite Structures*, 2012, vol. 94, pp. 415-422.

12. Carrera, E. Theories and finite elements for multilayered, anisotropic, composite plates and shells. *Archives of Computational Methods in Engineering*, 2002, vol. 9, pp. 1-60.

13. Carrera, E. Theories and finite elements for multilayered plates and shells: a unified compact formulation with numerical assessment and benchmarking. Archives of Computational Methods in Engineering, 2003, vol. 10, pp. 215-296.

14. Kulikov, G.M., Carrera, E. Finite deformation higher-order shell models and rigid-body motions. *International Journal of Solids and Structures*, 2008, vol. 45, pp. 3153-3172.

15. Kulikov, G.M., Plotnikova, S.V. Exact 3D stress analysis of laminated composite plates by sampling surfaces method. *Composite Structures*, 2012, vol. 94, pp. 3654-3663.

16. Kulikov, G.M., Plotnikova, S.V. Three-dimensional exact analysis of functionally graded laminated composite plates. *Advanced Structured Materials*, 2015, vol. 45, pp. 223-241.

17. Kulikov, G.M., Plotnikova, S.V. A sampling surfaces method and its implementation for 3D thermal stress analysis of functionally graded plates. *Composite Structures*, 2015, vol. 120, pp. 315-325.

18. Kulikov, G.M., Plotnikova, S.V. Three-dimensional analysis of metal-ceramic shells by the method of sampling surfaces. *Mechanics of Composite Materials*, 2015, vol. 51, pp. 455-464.

19. Kulikov, G. M., & Plotnikova, S. V. Sampling surfaces formulation for thermoelastic analysis of laminated functionally graded shells. *Meccanica*, 2016, vol. 51, pp. 1913-1929.

20. Burden, R.L., Faires, J.D. *Numerical analysis*. Ninth ed. Boston: Brooks/Cole, Cengage Learning, 2010.

21. Sze, K.Y., Chan, W.K., Pian, T.H.H.. An eight-node hybrid-stress solid-shell element for geometric non-linear analysis of elastic shells. *International Journal for Numerical Methods in Engineering*, 2002, vol. 55, pp. 853-878.

22. Park, H.C., Cho, C., Lee, S.W. An efficient assumed strain element model with six dof per node for geometrically non-linear shells. *International Journal for Numerical Methods in Engineering*, 1995, vol. 38, pp. 4101-4122.

23. Hoa, S.V., Feng, W. *Hybrid finite element method for stress analysis of laminated composites*. New York: Springer Science, 1998.

24. Kulikov, G.M., Plotnikova, S.V. A method of solving three-dimensional problems of elasticity for laminated composite plates. *Mechanics of Composite Materials*, 2012, vol. 48, pp. 15-26.

25. Kulikov, G.M., Mamontov, A.A., Plotnikova, S.V., Kulikov, M.G., Mamontov, S.A. Sampling surfaces formulation for functionally graded and laminated composite shells. *Advanced Materials and Technologies*, 2016, no. 1, pp. 61-66.

26. Kulikov, G.M., Plotnikova, S.V. A hybrid-mixed four-node quadrilateral plate element based on sampling surfaces method for 3D stress analysis. *International Journal for Numerical Methods in Engineering*, 2016, vol. 108, pp. 26-54.

27. Kulikov, G.M., Plotnikova, S.V. Hybrid-mixed ANS finite elements for stress analysis of laminated composite structures: Sampling surfaces plate formulation. *Computer Methods in Applied Mechanics and Engineering*, 2016, vol. 303, pp. 374-399.

28. Washizu, K. *Variational methods in elasticity and plasticity*. Third ed. Oxford: Pergamon, 1982.

29. Hughes, T.J.R., Tezduyar, T.E. Finite elements based upon Mindlin plate theory with particular reference to the four-node bilinear isoparametric element. *Journal of Applied Mechanics*, 1981, vol. 48, pp. 587-596.

30. Bathe, K.J., Dvorkin, E.N. A four-node plate bending element based on Mindlin/Reissner plate theory and a mixed interpolation. *International Journal for Numerical Methods in Engineering*, 1985, vol. 21, pp. 367-383.

31. Pian, T.H.H., Sumihara, K. Rational approach for assumed stress finite elements. *International Journal for Numerical Methods in Engineering*, 1984, vol. 20, pp. 1685-1695.

32. Simo, J.C., Fox, D.D., Rifai, M.S. On a stress resultant geometrically exact shell model. Part II: The linear theory; computational aspects. *Computer Methods in Applied Mechanics and Engineering*, 1989, vol. 73, pp. 53-92.

33. Simo, J.C., Rifai, M.S., Fox, D.D. On a stress resultant geometrically exact shell model. Part IV: Variable thickness shells with through-the-thickness stretching. *Computer Methods in Applied Mechanics and Engineering*, 1990, vol. 81, pp. 91-126.

34. MacNeal, R.H., & Harder, R. L. A proposed standard set of problems to test finite element accuracy. *Finite Elements in Analysis and Design*, 1985, vol. 1, pp. 3-20.